Journal of Power Sources 193 (2009) 515–522

Contents lists available at ScienceDirect

Journal of Power Sources

journal homepage: www.elsevier.com/locate/jpowsour

Electrochemical analysis of polymer electrolyte membrane fuel cell operated with dry-air feed

Hee-Tak Kim*, Kah-Young Song, Tatyana V. Reshetenko[1], Sang-Il Han, Tae-Yoon Kim, Sung-Yong Cho, Myoung-Ki Min, Geun-Seok Chai, Soon-Cheol Shin

Samsung SDI Co. Ltd., 575 Shin-dong, Yeongtong-gu, Suwon-si, Gyeonggi-do 443-391, Republic of Korea

ARTICLE INFO

Article history:
Received 5 February 2009
Received in revised form 2 April 2009
Accepted 8 April 2009
Available online 23 April 2009

Keywords:
Polymer electrolyte membrane fuel cell
Dry-air feed
Resistance
Relative humidity
Electrochemical area
Catalyst layer

ABSTRACT

Electrochemical analysis of a commercial polymer electrolyte membrane fuel cell (PEMFC), operated at varying cathode relative humidity (RH) and current density, has been conducted to understand the factors that affect power performance when the PEMFC is operated with a dry-air feed. With a change in the cathode RH from 80 to 4%, the electrochemical area and double-layer capacitance of the cathode are reduced by 9 and 8%, respectively. This indicates that exclusion of the catalyst layer (CL) of the cathode from proton access occurs to some extent at low RH. It does not, however, explain the observed increase in activation loss. For the dry-air feed, the ionic resistances of the membrane and cathode CL are comparable in magnitude. Impedance analyses show that drying of the cathode at low RH and low current density leads not only to an increase in the ionic resistance of the CL, but also to increases in both charge-transfer and mass-transfer resistances. The simultaneous decrease in all the resistance components with decrease in the air permeability of the cathode diffusion layer highlights the importance of cathode design for operation with dry-air feed.

1. Introduction

The operation of polymer electrolyte fuel cells (PEMFCs) at reduced- or zero-relative humidity (RH) without an external humidifier is a crucial step towards simplifying the system because the humidifier, which occupies space and requires a heat supply, causes a decrease in system efficiency. Given that hydrogen-generating units based on steam reforming or sodium borohydride can generate humidified hydrogen, a PEMFC system without external humidifier can be established if operation with dry-air is possible [1,2]. Previous research has shown that a reduction in cathode humidity has a profound effect on cell performance compared with reduction in the anode humidity [3], namely, it has detrimental effects on the steady and dynamic performances of the fuel cell [4]. The performance of a cell with dry feeds has been found to decline with both increase in operating temperature/flow of reactant gas and decrease in operating pressure [5].

It has been widely accepted that the drying of membranes gives rise to a large ohmic loss and hence low power performance. Consequently, most approaches aimed at solving the problem of operation with a dry-air feed have focused on creating new materials for conducting protons that either do not require water or have a reduced dependency on water [6–9]. Recently, the importance of water management for operation with dry-air has been stressed in several reports [4,6,10]. The use of a microporous layer with a low water-vapour permeability is found to enhance power performance with a dry-air feed [10]. The use of channel-less, self-draining fuel cells has also been suggested for auto-humidified operations [6]. Over a broad range of practical current densities, there are no water-supplementation requirements because the water produced at the cathode is sufficient to meet the water requirement of the membrane in a fuel cell [11].

Although the ionic resistance of the cell, including the contribution from the catalyst layer (CL), is a major source of performance losses in PEMFCs at low humidity, previous analyses of cell resistance have been directed primarily at the membrane resistance [12,13]. Because measurement of the ionic resistance of the CL is difficult, it is ignored. A recent publication, however, has addressed the importance of ionic resistance of CL for the operation of PEMFCs at 120 °C and reduced RH [14]. A decrease in the electrochemical area (ECA) caused by drying of cathode has also been stated to be a source of performance loss at low RH [5,15–18] but there are no reports of a quantitative analysis of the ECA under varying RH conditions.

In this study, the electrochemical characteristics of a commercial PEMFC membrane electrode assembly (MEA) have been investigated using current–voltage (*I–V*) polarization, cyclic voltammetry

* Corresponding author. Tel.: +82 31 210 7047; fax: +82 31 210 7374.
E-mail address: hee-tak.kim@samsung.com (H.-T. Kim).
[1] Current address: Hawaii National Energy Institute, University of Hawaii, Honolulu, USA.

0378-7753/$ – see front matter © 2009 Elsevier B.V. All rights reserved.
doi:10.1016/j.jpowsour.2009.04.027

(CV) and impedance spectroscopy, with varying values of cathode RH and current densities at a constant anode RH of 80%. The main objectives of this work are: (i) to clarify the dependency of the ECA and double-layer capacitance on cathode humidity and the influence of the change in ECA on power performance; (ii) to quantify the relative significance of the ionic resistance of the CL in comparison with that of the membrane; (iii) to investigate the relationships between cathode hydration, charge-transfer reaction and mass-transfer limitation when operated with a dry-air feed. The study aims to provide both a clearer understanding of the origin of power loss induced by reducing the cathode RH and useful information related to PEMFC designs to achieve high power performance in the absence of a cathode humidifier.

2. Experimental

2.1. Assembly of single cell

Single cells were assembled with a commercial catalyst-coated membrane of size 26 cm^2, based on Pt/C (cathode) and PtRu/C (anode), a pair of gas-diffusion media (31BC, SGL), a pair of Teflon gaskets, and a pair of graphite blocks, with triple serpentine flow fields for the reactants. The flow fields for the anode and cathode reactants were mirror images. The total Pt loading was less than 0.7 mg cm^{-2}. A perfluorinated ionomer was used as both the membrane and binder for the CL.

2.2. Measurement of I–V polarization

I–V polarization curves were obtained by stepping up the current density, allowing the cell to stabilize, and measuring the cell voltage. Two minutes were spent at each current density, with the cell voltage recorded every 2 s. The cell resistance was measured at each current density by means of the current-interrupt technique. For hydrogen, a constant mass-flow rate of 43.5 sccm was used for current densities below 200 mA cm^{-2}; above 200 mA cm^{-2}, a constant stoichiometry of 1.2 was employed. Airflow at a constant mass-flow rate of 215.6 sccm was used for current densities below 200 mA cm^{-2}; above 200 mA cm^{-2}, a constant stoichiometry of 2.5 was employed. The cell temperature was controlled at 60 °C. The RH of the dry-air feed was 4% at 60 °C.

2.3. CV studies

Cyclic voltammetry was performed on the single cell (using a SI 1287, Solarton Analytical potentiostat to determine the ECA and double-layer capacitance using at different cathode RH values. To obtain the CV curve of the cathode, it was considered as the working electrode and fed with nitrogen, whereas the anode that was fed with pure hydrogen functioned as both the counter and reference electrodes. Hydrogen was 80% humidified at the cell temperature of 60 °C. The RH of nitrogen was varied at 4, 10, and 80%. The potential was scanned between 0.08 and 0.80 V at various scan rates (20, 50, 80, and 100 mV s^{-1}).

2.4. Electrochemical impedance spectroscopy

Electrochemical impedance spectroscopy (EIS) was carried out to calculate the ionic resistances of the membrane and the CL, the charge-transfer resistance, and the mass-transfer resistance. The procedure was conducted in the frequency range of 10 kHz–100 mHz with 10 steps per decade using a potentiostat (SI 1287, Solartron Analytical), in conjunction with a frequency-response analyzer (SI 1255B, Solartron Analytical), a power booster (SI 1290, Solartron Analytical), and the software Zplot 2.6b developed by Scribner Associates Inc. The amplitude of the sinusoidal voltage signal did not exceed 10 mV. The cathode was used as a working electrode and the anode as a counter electrode. The counter electrode also served as a reference electrode, because the overpotential of hydrogen oxidation at the counter electrode is negligible.

3. Results and discussion

3.1. I–V polarization of PEMFC at various levels of cathode RHs

The cell voltage and current-interrupt resistance are shown in Fig. 1 as functions of the current density at 60 °C for three different cathode RHs of 4, 10, and 80%. The cell performance is significantly affected by the cathode RH. The power density at 0.7 V is selected to evaluate the cell performance. At 80% RH, the power density at 0.7 V is 290.8 mW cm^{-2}; at 10% RH, it is 253.4 mW cm^{-2}; and when a dry-air feed (4% RH) is used, the cell performance is 212.6 mW cm^{-2}. There is a sharp decrease in the cell performance with decrease in RH. With increasing current density, the current-interrupt resistances at 4 and 10% RH appear to decrease exponentially and approach constant values. At 80%, the current-interrupt resistance is not significantly dependent on current density. Throughout the entire range of current density, the current-interrupt resistance is greater for a lower cathode RH. For low cathode RHs of 4 and 10%, the water generated by the electrochemical reduction of oxygen serves to hydrate the MEA, resulting in a decrease of the current-interrupt resistance with current density.

At low current densities (below 100 mA cm^{-2}), the cell voltage increases with decrease in the cathode RH, as shown in the inset of Fig. 1. The higher cell voltage observed at a lower cathode RH in this range of current density does not imply a smaller activation loss at the lower cathode RH. In fact, the activation loss grows larger with decreasing RH, as discussed in Section 3.3. This behaviour is attributed to an increase in the open-circuit voltage (OCV) with decrease in cathode RH. According to the Nernst equation, thermodynamically, the theoretical OCV decreases with RH due to the higher water-vapour pressure. The OCV is 0.968, 0.949 and 0.928 when measured at 4, 10, and 80% RH, respectively.

3.2. Effect of cathode RH on ECA and double-layer capacitance

Many researchers expect that a dry environment can slow down oxygen-reduction reactions due to a reduction in the ECA in a dried CL [5,15–18]. In other words, a significant drying of the ionomers in CL disconnects the proton-transfer passage, and some catalyst

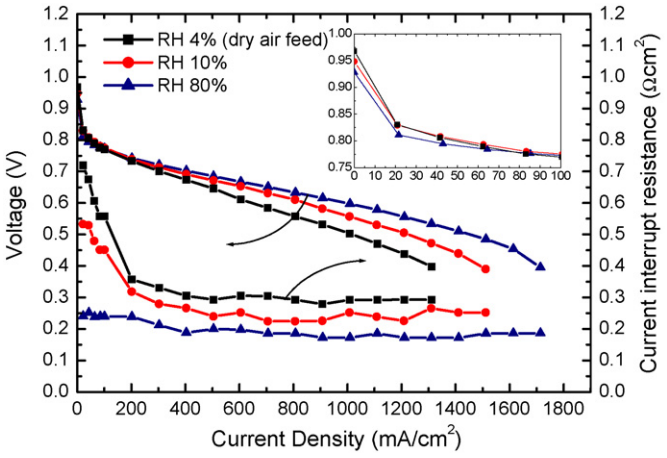

Fig. 1. Plot of cell voltage and current-interrupt resistance as function of current density at 60 °C for three different values of cathode RHs 4, 10, and 80% (anode RH: 80%; stoichiometry: 2.5 for cathode and 1.2 for anode).

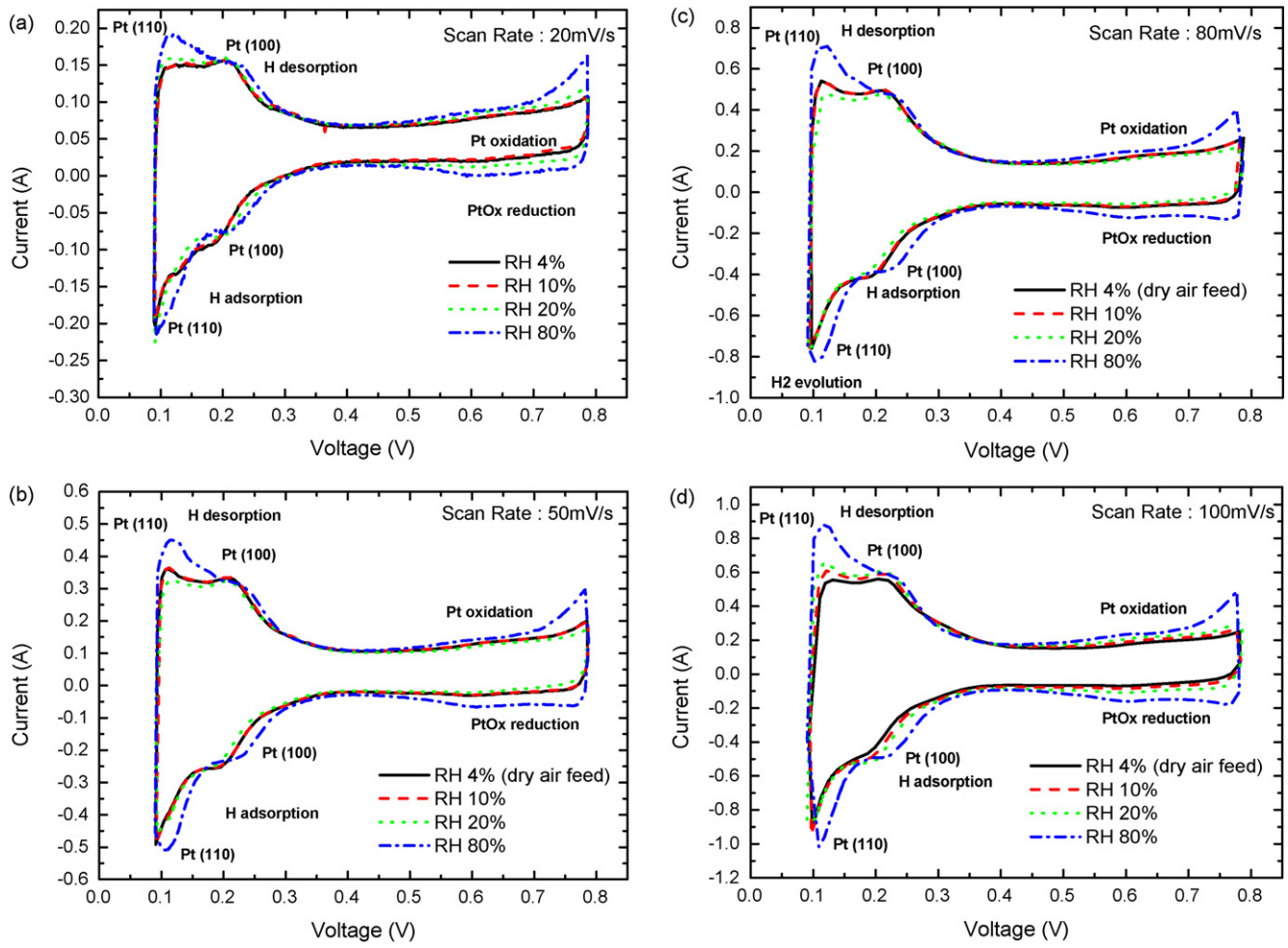

Fig. 2. Cyclic voltammograms measured at various cathode RHs and various scan rates (scan rates: (a) 20, (b) 50, (c) 80, and (d) 100 mV s^{-1}; cathode feed: nitrogen; anode feed: 80% RH hydrogen; cell temperature: 60 °C).

surfaces are isolated from proton access. The CV profile of the cell was therefore measured with varying cathode RHs to elucidate the effect of cathode RH on the cathode ECA. The cyclic voltammograms at various cathode RHs and scan rates are presented in Fig. 2. At all the scan rates, the current peaks due to H-adsorption at the Pt(1 0 0) and Pt(1 1 0) planes shift to higher voltages (by about 30 mV) with increase in the cathode RH from 4 to 80%. This indicates that proton-transfer to the Pt surface is moderately hindered at low RHs. The potential for H-desorption is insensitive to cathode RH because H-desorption is not associated with proton diffusion. At higher RH values, both Pt-oxidation and the Pt-oxide-reduction currents in the 0.55–0.8 V range are strong, indicating that the concentration of water near the Pt surface is high.

The cathode ECA is calculated from the average of the charges from H-adsorption and H-desorption after subtracting the charge from the double-layer charging. The changes appearing in the ECA with varying scan rates for different cathode RHs are indicated in Fig. 3. Irrespective of the range of cathode RH, the ECA tends to decrease with increase in scan rate. This is logical because H-adsorption is affected by the rate at which the proton is delivered to the Pt surface. At 20 mV s^{-1}, the ECA is reduced by 11% with decrease in the cathode RH from 80 to 4%. The difference in ECA values between the high RH and the low RH conditions increases with scan rate, confirming that the proton-diffusion rate influences the ECA values. To eliminate the effect of the scan rate on ECA, the plots are extrapolated to a scan rate of 0 mV s^{-1}. This leads to a 9% reduction in the ECA with change in RH from 80 to 4%, which indicates that the loss of active catalyst surface occurs by its isolation from proton access due to partial drying of the cathode.

Double-layer capacitance is another parameter indicative of the measure of the access of the interface to protons. From the dependency of the capacitive charging current (I_c) at 0.4 V on the scan

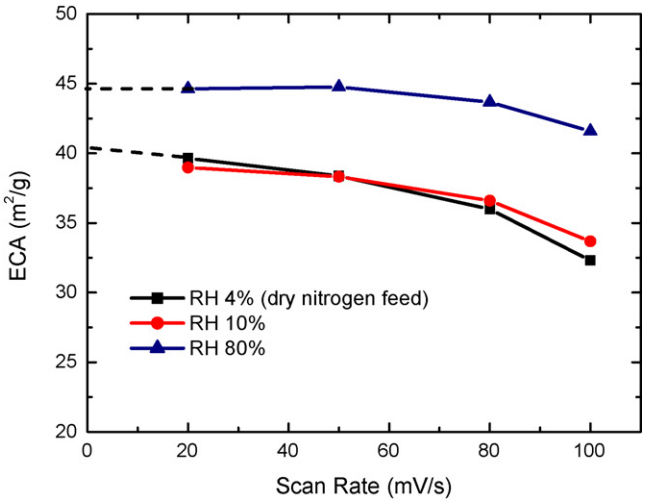

Fig. 3. Plot of ECA as function of scan rate for various values of cathode RH.

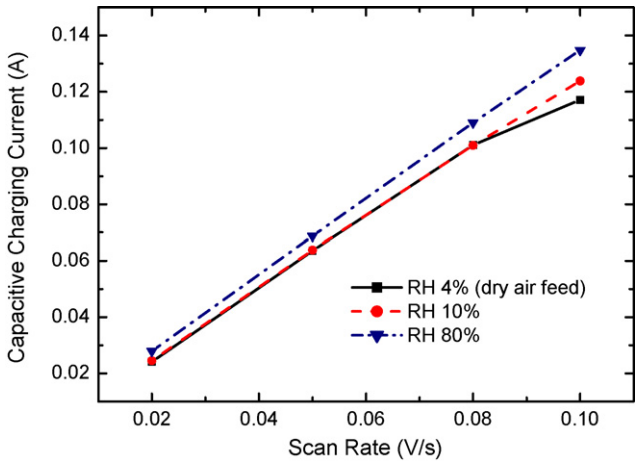

Fig. 4. Plot of capacitive charging current as function of scan rate for various cathode RHs.

rate, the double-layer capacitance (C_{dl}) can also be determined. With increase in scan rate, I_c linearly increases, according to the following relationship.

$$I = C_{dl}\frac{dV}{dt} \quad (1)$$

A plot of I_c as a function of the scan rate for various cathode RHs is presented in Fig. 4. As expected, a linear relationship is observed for all the RH conditions tested. The values of C_{dl} are quantified from the slope and are listed in Table 1. The C_{dl} decreases by 8% with decrease in RH from 80 to 4%, which is in good agreement with the ECA results. The influence of the ECA loss on power performance is discussed in the next section in conjunction with an impedance analysis.

3.3. Impedance analyses of cell at various cathode RHs and current densities

The impedance spectra of the cell at various cathode RHs and current densities are provided in Fig. 5. The impedance spectra are characterized by the following features: (i) the intercept in the high-frequency domain on the Z' axis, which corresponds to the ohmic resistance (R_m); (ii) the linear region starting from the intercept on the Z' axis, which represents the contribution from ionic conduction through the CL; (iii) the semicircle at higher frequencies, originating from the charge-transfer process (the cathodic oxygen-reduction); and (iv) the semicircle at lower frequencies, originating from the mass-transfer processes, with contributions from proton-diffusion, gas-diffusion, or both [19–22]. With decreasing frequency, these contributions are evident in the following order: ionic conduction through the membrane, ionic conduction through the CL, charge-transfer reaction, and mass-transfer process. Because oxidation of hydrogen is much faster than reduction of oxygen, the contribution from the anode is generally ignored.

At 4 and 10% RHs, the R_m decreases markedly with current density, as shown in Fig. 5(a) and (b). At 80% RH, however, the ohmic resistance does not change with current density (Fig. 5(c)). The values for R_m under various RH conditions are listed in Table 1. The indicated value of R_m includes the ionic resistance of the membrane and any electronic resistance of the cell. Because the electronic resistance does not change with the cathode RH and current density, the observed change in R_m exclusively reflects the effect of a physicochemical change in the membrane.

The plot of Z'' is provided as a function of $Z' - R_m$ in Fig. 6, which magnifies the linear region at high frequencies. In the linear region, Faradaic processes are not significant, and the effects of both

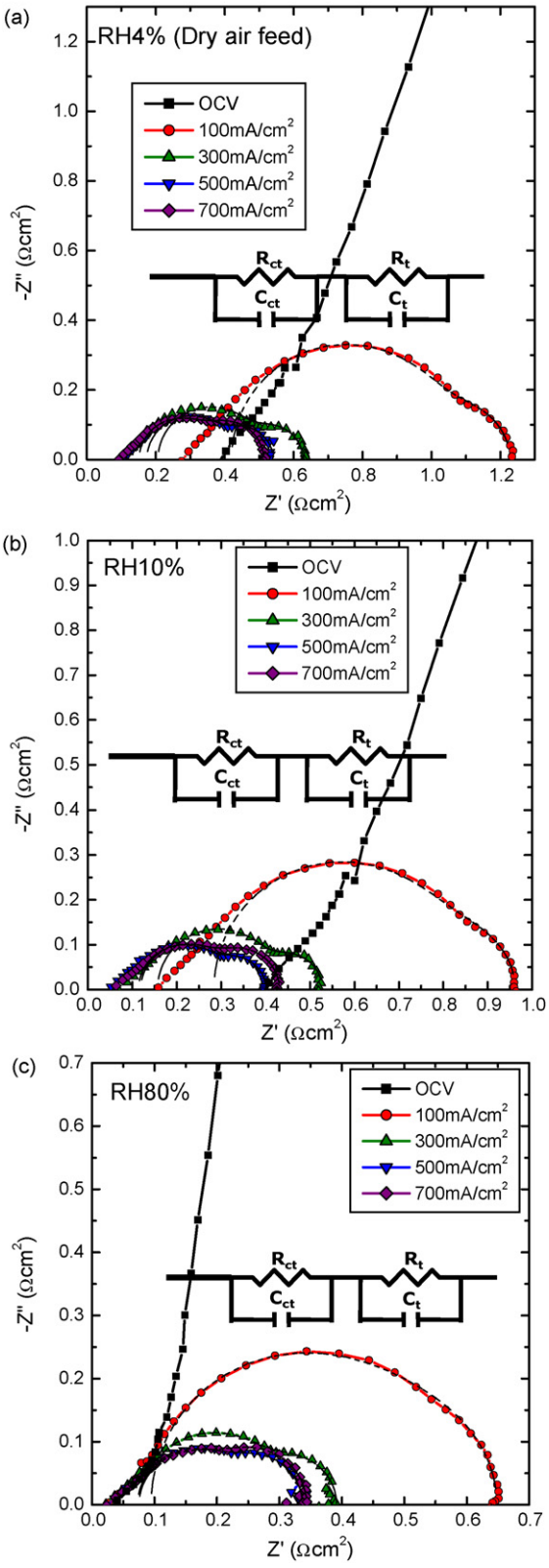

Fig. 5. Impedances of cell at various current densities at cathode RH values of (a) 4%, (b) 10%, and (c) 80% (cell temperature: 60 °C).

double-layer charging and proton-transfer through the CL dominate the overall response, which is typical of a porous electrode [23]. The subtraction of R_m from Z' is aimed at focusing on proton-transfer through the CL. Considering 4 and 10% RH, a deviation from the 45° line is observed at the OCV and low-current densities. With

Table 1
Electrochemical parameters of cell at various cathode RHs and current densities, as determined from CV and EIS analyses.

Cathode RH (%)	Current density (mA cm^{-2})	R_m (Ω cm^2)	R_{cl} (Ω cm^2)	R_{ct} (Ω cm^2)	R_{tr} (Ω cm^2)	λ_p/l	C_{dl} (F cm^{-2})	C_{ct} (F cm^{-2})	C_{tr} (F cm^{-2})
4	0 (OCV)	0.389	0.400				0.045		
	100	0.278	0.217	0.625	0.182	1.697		0.015	0.513
	300	0.102	0.120	0.275	0.146	1.514		0.025	0.527
	500	0.104	0.095	0.222	0.145	1.519		0.024	0.392
	700	0.093	0.067	0.195	0.171	1.707		0.027	0.251
10	0 (OCV)	0.400	0.395				0.048		
	100	0.155	0.170	0.531	0.147	1.768		0.019	0.542
	300	0.074	0.102	0.252	0.120	1.571		0.023	0.644
	500	0.046	0.085	0.177	0.110	1.445		0.028	0.451
	700	0.056	0.076	0.168	0.144	1.488		0.026	0.278
80	0 (OCV)	0.034	0.087				0.052		
	100	0.024	0.073	0.410	0.144	2.370		0.032	0.371
	300	0.021	0.064	0.204	0.110	1.784		0.032	0.545
	500	0.025	0.053	0.145	0.119	1.652		0.035	0.329
	700	0.024	0.049	0.126	0.143	1.603		0.038	0.237

increasing current density, the angle approaches the 45° line. For 80% RH, however, no such deviation is observed. The value of 45° originates from the assumption that the proton-transfer resistance is uniformly distributed across the CL [24]. Recently, Lee and Pyun [25] asserted that the positive deviation from 45° can be explained in terms of a non-uniform distribution of ionic resistance across the CL. Thus, assuming that the distribution of ionic resistance follows an exponential function of the distance from the membrane, the appearance of an angle greater than 45° can be successfully explained. The fact that the positive deviation is larger for lower values of RH and current density strongly suggests that the degree of hydration of the ionomer is not uniform across the CL under these conditions. Because the anode side is highly hydrated, the degree of hydration can be decreased with increasing distance from the membrane|cathode interface. At high values of RH and current density, the non-homogeneity is relieved, resulting in an approach towards the 45° angle.

The ionic resistance of the cathode (R_{cl}) can be determined from the impedance in the linear region, and the C_{dl} of the cathode can be determined from the CV analysis. The impedance in the linear region can be expressed in terms of the R_{cl} and C_{dl} of the cathode and frequency (ω) as follows [24]:

$$|Z| = \sqrt{\frac{R_{cl}}{C_{dl}}\omega^{-1/2}} \quad (2)$$

The ratio of R_{cl} and C_{dl} is determined by fitting the linear region with Eq. (2). The C_{dl} is obtained from the relation between I_c and scan rate, as described in Section 3.2. The R_{cl} is subsequently calculated.

The R_m and R_{cl} at various current densities are compared in Fig. 7. For 4 and 10% RHs, both R_m and R_{cl} exponentially decrease with current density, indicating that both the membrane and the cathode are considerably dehydrated at low current densities. The R_{cl} is comparable with, or even greater than, the R_m at 4 and 10% RH values. This strongly suggests that the ionic resistance of the CL is as important as the membrane resistance in the cell design for low humidity operation, although it has not been considered in many analyses.

To quantify the contributions from the oxygen-reduction reaction and mass-transfer limitation, fitting of the data to a circuit model has been carried out. The oxygen-reduction reaction is described by the parallel combination of charge-transfer resistance (R_{ct}) and pseudo-double-layer capacitance (C_{ct}). The mass-transfer limitation is also expressed by the parallel combination of mass-transfer resistance (R_{tr}) and a capacitance (C_{tr}). The circuit model used in the study is shown in Fig. 4. The C_{ct} differs from the C_{dl} used in the transmission line–element model. Because double-layer charging during the course of the electrochemical reaction is not a static, but a dynamic, process [23], the C_{ct} is the result of the repeated dynamic processes in which the proton is adsorbed on the Pt surface and is subsequently removed by the electrochemical reaction.

The results of the fitting of the circuit model to the semicircles are presented in Fig. 5 as solid lines. A reasonable fit is observed for all the impedances. The values for R_{ct}, C_{ct}, R_{tr}, and C_{tr} determined from the fitting are listed in Table 1. R_{ct} and R_{tr} are plotted as functions of the current density for 4, 10, and 80% RH in Fig. 8. The R_{ct} rapidly decreases with current density irrespective of cathode RH, because the increased overpotential renders the reaction faster. The R_{tr} decreases with current density but increases, again at 700 mA cm^{-2}, irrespective of the cathode RHs. Both charge-transfer and mass-transport resistances are larger for lower cathode RH values.

The overpotential for oxygen-reduction corresponds to the product of R_{ct} and current density. At 100 mA cm^{-1}, the overpotentials based on the magnitude of R_{ct} are 62.9, 53.5 and 41.3 mV for 4, 10, and 80% RH, respectively, and at 300 mA cm^{-1} are 83.3, 76.2 and 61.8 mV for 4, 10, and 80% RH, respectively. The increase in overpotential after reduction of the RH from 80 to 4% amounts to 21.6 and 21.5 mV at 100 and 300 mA cm^{-2}, respectively. Given that the Tafel slope for the oxygen-reduction reaction in a H_2–air fuel cell at 60 °C is 68 mV [26], the voltage loss of 22 mV amounts to a reduction of the ECA to 47.5% of the initial value, assuming that the exchange-current density is independent of RH. By contrast, the ECA loss due to isolation from proton access is found to be only 9%, as shown in Section 3.2. Therefore, the effect of cathode RH on R_{ct} cannot be explained in terms of a change in the ECA.

It is feasible that the slow proton transport through the cathode CL leads to a reduction in the reaction zone. Only a limited region of the cathode CL, starting from the membrane|CL interface, would be used when the proton-transfer rate is slower than the proton-consumption rate. To investigate how strongly the proton-transport rate affects the reaction of oxygen-reduction, the concept of reaction-penetration depth, suggested by Eikerling and Kornyshev [24], has been applied. The reaction-penetration depth (λ_p) is indicative of the portion of CL where protons can be delivered at a given reaction rate and is defined as:

$$\lambda_p = \sqrt{\frac{R_{cl}}{R_{ct}} l_e} \quad (3)$$

where l_e corresponds to the thickness of the CL. When $\lambda_p/l \gg 1$, proton-transfer through CL proceeds at a much faster rate than the electrochemical reaction, and the entire CL can be used for the process. In the case where $\lambda_p/l < 2$, the proton-transfer limitation is strong and the electrochemical reaction is concentrated on a limited region of the membrane|CL interface.

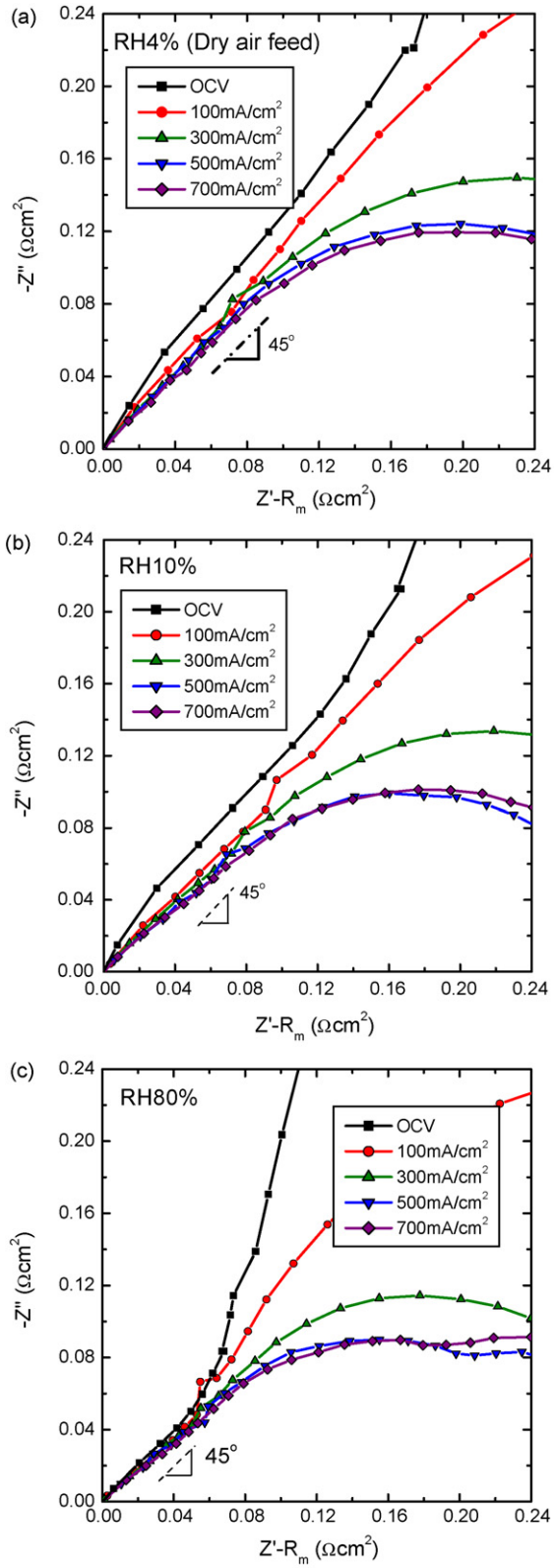

Fig. 6. Plot of Z'' as function of $Z' - R_m$ for impedances of cell at cathode RH of (a) 4%, (b) 10%, and (c) 80% (cell temperature: 60 °C).

The change of λ_p/l_e with current density for various cathode RHs is given in Fig. 9. At a low current density of 100 mA cm^{-2}, the λ_p/l_e is 1.70, 1.77 and 2.37 for cathode RH values of 4, 10, and 80%, respectively. The small values of λ_p/l_e at 4 and 10% RHs show that proton-transfer at these low RHs limits the charge-transfer reaction more significantly compared with that at 80% RH. At high current densities (>500 mA cm^{-2}), the values for λ_p/l are in the range of 1.4–1.7, and the difference in λ_p/l with cathode RH is relatively small. This indicates that the proton-transfer limitation is considerable at high current densities, irrespective of cathode RH.

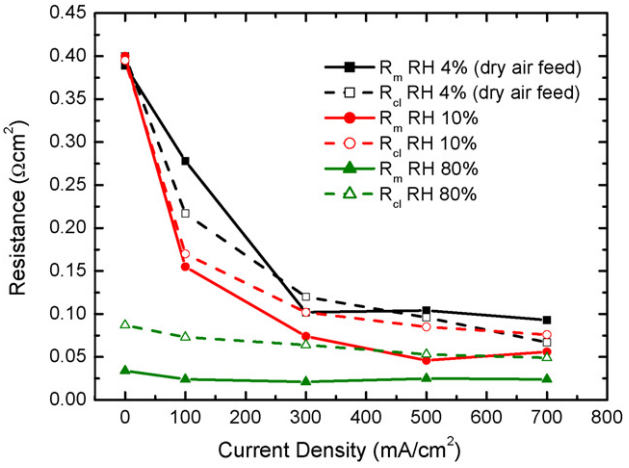

Fig. 7. Plots of R_m and R_{cl} as function of current density for various cathode RHs.

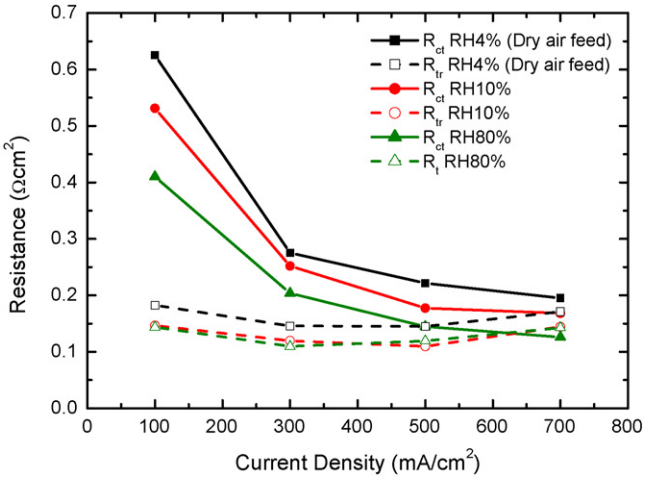

Fig. 8. Plots of R_{ct} and R_{tr} as function of current density for various cathode RHs.

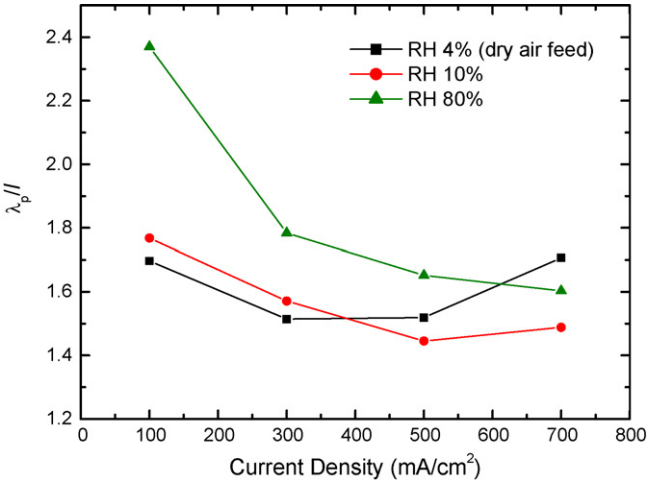

Fig. 9. Plot of reaction-penetration depth as function of current density for various cathode RHs.

Considering that the differences in R_{ct} and λ_p/l_e between 80 and 4% RH at 100 mA cm^{-2} are much greater than those at higher current densities, it is reasonable to conclude that slow proton-transfer is responsible for the large charge-transfer resistance at 100 mA cm^{-2} when a dry-air feed is applied.

The dependency of C_{ct}, the pseudo-double-layer capacitance, on cathode RH and current density supports a short reaction-penetration depth at low values of RH and current density. For low RHs of 4 and 10%, the C_{ct} values at 100 mA cm^{-2} are relatively small compared with those at high current densities. At a high RH of 80%, however, C_{ct} has shown weak dependency on current density (Table 1). Recognizing that C_{ct} is an increasing function of the area of the ionically active surface, the relatively small value for C_{ct} reconfirms limited usage of the CL. On the other hand, the higher values of C_{ct} compared with those of C_{dl} are indicative of pseudocapacitive behaviour. The repeating processes of proton consumption by oxygen-reduction and replenishment of the Pt surface with protons leads to the higher values of C_{ct}.

The appearance of a minimum for R_{tr} at an intermediate current density suggests that the origin of the mass-transport limitations at low and high current densities is different. At high current density, local flooding of the cathode by the water released by electroosmosis and electrochemical production of water is only to be expected. It is less probable, however, that the mass-transfer limitation at low current density and low RH originates from water flooding; rather, the phenomenon could be due to a shortage of either oxygen or protons. Oxygen permeability of dry Nafion is known to be an order of magnitude lower than that of wet Nafion, because oxygen diffuses more readily through water cluster regions than through the hydrophobic polymeric phase. Broka and Ekdunge [27] employed gas chromatography to study oxygen permeability across Nafion membranes. Their study found that at 85 °C, the oxygen permeability is 9.0×10^{-12} mol (cm s at)$^{-1}$ for a recast Nafion 117 membrane at 100% RH. The permeability declined to 3.0×10^{-12} mol (cm s at)$^{-1}$ under completely dry conditions. Gode et al. [28] used a microelectrode coated with a Nafion film to measure oxygen permeability, and found that at 60 °C, oxygen permeability for 95% RH is 5.0×10^{-12} mol (cm s at)$^{-1}$, but declines to 2.5×10^{-12} mol (cm s at)$^{-1}$ at 35% RH. Sakai et al. [29] reported that air permeability increases with water content, inferring that gas-diffusion through the water-cluster phase is facilitated at high RH. By contrast, Paganin et al. [22] suggested that the low frequency arc is due to a proton-transfer process in the membrane, but the conclusion was tentative.

To elucidate the origin of the low-frequency resistance at low RH and low current density, the impedances at varying flow rates of dry-air feed were investigated. An increased airflow would help oxygen transport through the cathode. On the other hand, it would render the membrane and the cathode dry and thereby lead to an increase in both the membrane resistance and the ionic resistance of the CL cathode. The change of impedance of the cell with increase in flow rate is shown in Fig. 10. The process described above determines the values for R_m, R_{cl}, R_{ct}, and R_t; plots of these resistances as a function of the air stoichiometry are displayed in Fig. 11. R_m increases from 0.175 to 0.362, and R_{cl}, from 0.160 to 0.329, with an increase in air stoichiometry from 2.5 to 5.0. This indicates that drying of the membrane and the cathode CLs is due to enhanced water removal and an increase in air stoichiometry. R_{ct} behaves similarly R_m and R_{cl}, which reconfirms that the ionic transport rate through the cathode CL largely determines the oxygen-reduction rate. Interestingly, R_{tr} is virtually unaffected by changes in air stoichiometry. If it is associated with proton limitation, it should increase with air stoichiometry. The invariance of R_{tr} with air stoichiometry indicates that the resistance shown at low cathode humidity and low current density appears to arise from the process of oxygen diffusion. The increase of air stoichiometry accelerates diffusion of

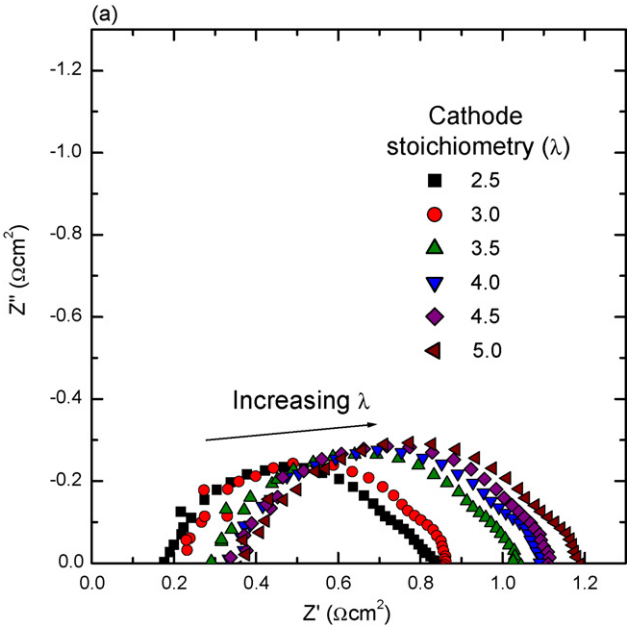

Fig. 10. Impedances of cell with dry-air feed at current density of 100 mA cm^{-2} at various air stoichiometry (cell temperature: 60 °C).

air through pores in the cathode and reduces air diffusion through the ionomer phase. These two opposite effects may result in the apparent insensitivity of R_{tr} to air stoichiometry.

Compared with the corresponding resistances at 80% RH, all the resistances (R_m, R_{cl}, R_{ct}, and R_{tr}) at 4% RH jump dramatically (Table 1) and thereby suggest that all these processes together are responsible for the decrease in performance with dry-air feed. Because hydration of the ionomer in the cathode CL strongly influences R_{cl}, R_{ct}, and R_{tr}, as shown above, a design for better cathode hydration would be the most effective strategy to enhance power performance, rather than a sole reliance on improving membrane hydration by structural modification of the membrane.

The importance of cathode hydration for operation with dry-air feed is highlighted by a comparison of the values of R_m, R_{cl}, R_{ct}, and R_{tr} for the two cathode-diffusion layers (31BC and 24BC) with different air permeabilities, as shown in Fig. 12. The air permeabilities of 31BC and 24BC are 2.0 and 0.6 cm^3 cm^{-2} s^{-1}, respectively. The

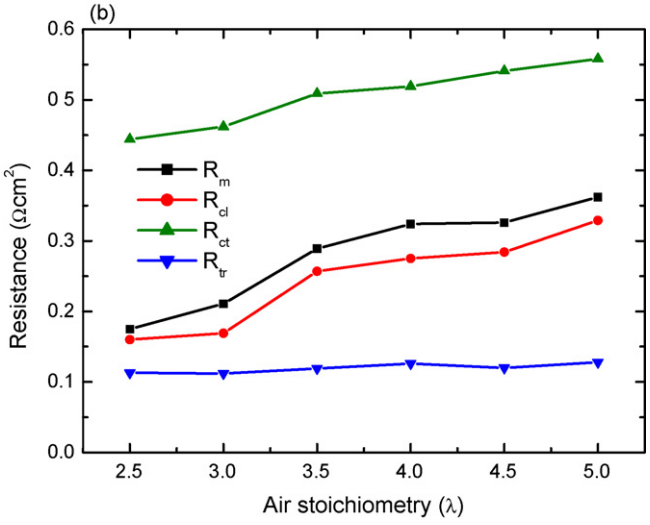

Fig. 11. Plots of R_m, R_{cl}, R_{ct}, and R_{tr} (measured at current density of 100 mA cm^{-2}) as function of air stoichiometry at cathode RH of 4% (cell temperature: 60 °C).

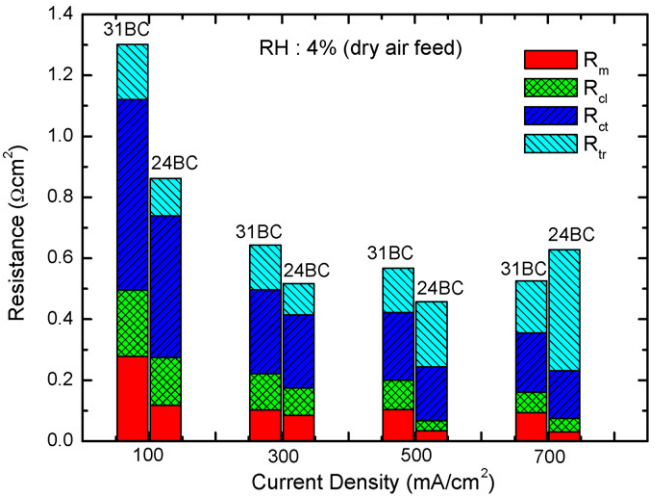

Fig. 12. Comparison between resistance components of 31BC and 24BC at various current densities.

resistance values for 24BC have been determined with the same impedance analyses described above. Water-vapour permeability is expected to be lower for 24BC based on the air permeability data. The retarded removal of water-vapour would be beneficial to cathode hydration, but it would be, simultaneously, prone to water flooding. As shown in Fig. 12, 24BC has greatly reduced R_m and R_{cl} compared with 31BC, as expected, and is more effective for cathode hydration, irrespective of current density. At 100 and 300 mA cm^{-2}, R_{tr} is smaller for 24BC despite the lower air permeability. This observation offers further confirmation that cathode dehydration mainly influences the mass-transfer resistance appearing at low current density. At 500 and 700 mA cm^{-2}, 24BC possesses a larger R_{tr} than 31BC probably due to severe water flooding. The impedance analysis also supports the approach suggested by Yoshikawa et al. [10], who introduced a diffusion layer with low water-vapour permeability to assist cathode hydration and, consequently, observed a substantial improvement in power performance.

4. Conclusions

Electrochemical analysis of a commercial PEMFC single cell operated at 60 °C with varying cathode RH and current density at a constant anode RH of 80% has been carried out to identify the factors that affect power performance when the PEFMC is operated with a dry-air feed. Three major observations have been made. First, the ECA and double-layer capacitance are weakly dependent on the cathode RH; but the behaviour is not sufficient to explain the observed power loss. Second, the ionic resistance of the CL is comparable with that of the membrane for dry-air feed. Third, at low RH and low current density, drying of the cathode influences not only the charge-transfer resistance but also the mass-transfer resistance. These results stress the importance of improving the cathode design for better hydration. For example, the use of a diffusion layer with low air permeability reduces all the resistance components at low current densities with a dry-air feed due to enhanced cathode hydration.

References

[1] S.-H. Ge, X.-G. Li, I.-M. Hsing, J. Electrochem. Soc. 151 (2004) B523.
[2] Y. Cai, J. Hu, H. Ma, B. Yi, H. Zhang, Electrochim. Acta 51 (2006) 6361.
[3] Q. Yan, H. Toghiani, J. Wu, J. Power Sources 158 (2006) 316.
[4] Q. Yan, H. Toghiani, H. Causey, J. Power Sources 161 (2006) 492.
[5] J. Zhang, Electrochim. Acta 52 (2007) 5095.
[6] W.H.J. Hogarth, J.C. Diniz da Costa, G.Q. Lu, J. Power Sources 142 (2005) 223.
[7] O. Savadogo, J. Power Sources 127 (2004) 135.
[8] T.M. Thampan, N.H. Jalani, P. Choi, R. Datta, J. Electrochem. Soc. 152 (2005) A316.
[9] C. Yang, P. Costamagna, S. Srinivasan, J. Benziger, A.B. Bocarsly, J. Power Sources 103 (2001) 1.
[10] Y. Yoshikawa, T. Matsuura, M. Kato, M. Hori, J. Power Sources 158 (2006) 143.
[11] D.M. Bernardi, M.W. Verbrugge, J. Electrochem. Soc. 139 (1992) 2477.
[12] F.N. Büchi, G.G. Scherer, J. Electroanal. Chem. 404 (1996) 37.
[13] B. Andreaus, G.G. Scherer, Solid State Ionics 168 (2004) 311.
[14] X. Hu, H.R. Kunz, J.M. Fenton, Electrochim. Acta 52 (2007) 3525.
[15] M. Watanabe, H. Uchida, M. Emori, J. Phys. Chem. B 102 (1998) 3129.
[16] Z. Qi, A. Kaufman, J. Power Sources 109 (2002) 38.
[17] F.N. Buchi, S. Srinivasan, J. Electrochem. Soc. 144 (1997) 2767.
[18] C. Song, Y. Tang, J.L. Zhang, J. Zhang, H. Wang, J. Shen, S. McDermid, P. Kozak, Electrochim. Acta 52 (2007) 2552.
[19] J. Perez, J. Electrochem. Soc. 145 (1998) 2307.
[20] T.E. Springer, T.A. Zawodzinski, M.S. Wilson, S. Gottesfeld, J. Electrochem. Soc. 143 (1996) 587.
[21] T.J.P. Freire, E.R. Gonzalez, J. Electroanal. Chem. 503 (2001) 57.
[22] V.A. Paganin, C.L.F. Oliveira, E.A. Ticianelli, T.E. Springer, E.R. Gonzalez, Electrochim. Acta 43 (1998) 3761.
[23] A. Parthasarathy, B. Dave, S. Srinivasan, A.J. Appleby, J. Electrochem. Soc. 139 (1992) 1634.
[24] M. Eikerling, A.A. Kornyshev, J. Electroanal. Chem. 475 (1999) 107.
[25] S.-J. Lee, S.-I. Pyun, Electrochim. Acta 52 (2007) 6525.
[26] A.J.-J. Kadjo, P. Brault, A. Caillard, C. Coutanceau, J.-P. Garnier, S. Martemianov, J. Power Sources 172 (2007) 613.
[27] K. Broka, P. Ekdunge, J. Appl. Electrochem. 27 (1997) 117.
[28] P. Gode, F. Jaouen, G. Lindbergh, A. Lundblad, G. Sundholm, Electrochim. Acta 48 (2003) 4175.
[29] T. Sakai, H. Takenaka, N. Wakabayashi, Y. Kawami, E. Torikai, J. Electrochem. Soc. 132 (1985) 1328.